

Appendix PDF

An inter-dimer allosteric switch controls NMDA receptor activity

Jean-Baptiste Esmenjaud, David Stroebel, Kelvin Chan, Teddy Grand, Mélissa David, Lonnie P. Wollmuth, Antoine Taly and Pierre Paoletti

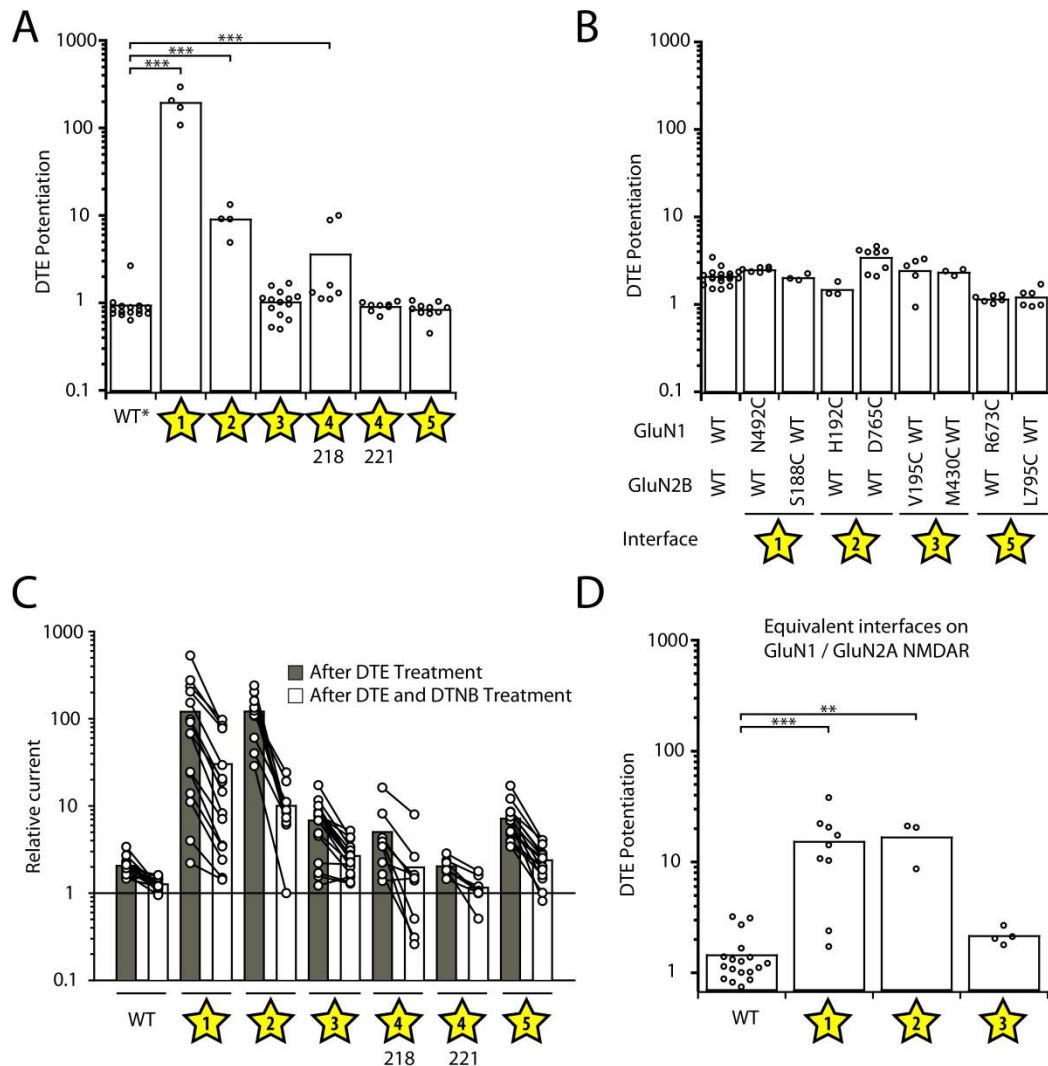
Corresponding authors: pierre.paoletti@ens.fr, antoine.taly@ibpc.fr

Appendix includes:

Appendix Figures S1-8

Appendix Tables S1-5

Appendix Movie Legends S1-2



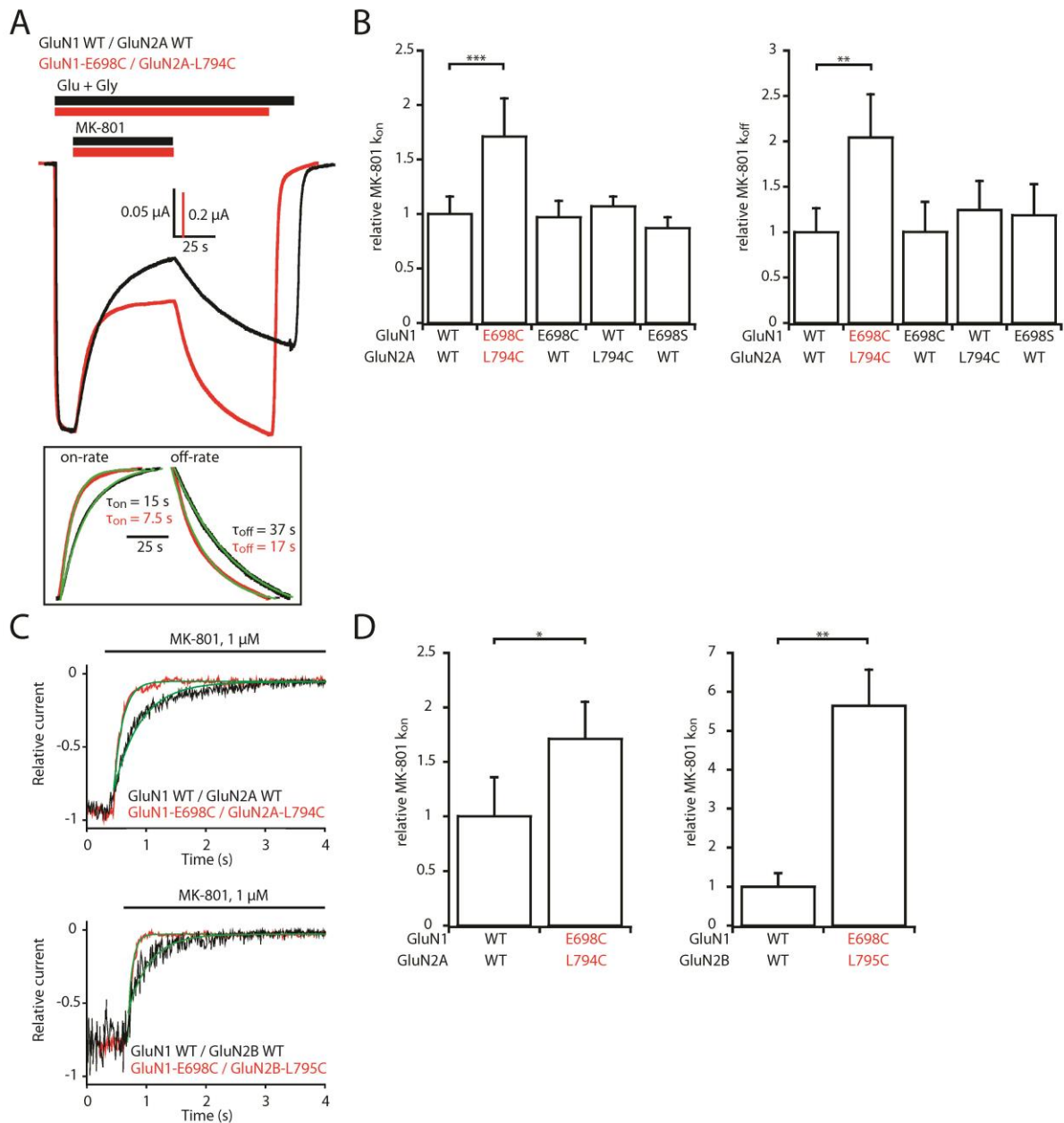
Appendix Figure S1: Effects of redox treatments on NMDAR activity.

(A) Summary of the DTE-induced potentiation of wild-type (WT) and double cysteine mutant receptors using the GluN1* subunit as background. GluN1* represents the GluN1 subunit with the two endogenous cysteines C744 and C798 mutated to alanine (C744A C798A). Because of the absence of the endogenous C744-C798 disulfide bridge, WT GluN1*/GluN2B NMDARs are redox insensitive. Yellow stars and their numbers indicate different inter-domain and inter-layer interfaces as depicted in Figure 1A.

(B) Summary of the DTE-induced potentiation of wild-type (WT) and single-cysteine control mutants.

(C) Change in current amplitude after reduction by DTE and subsequent oxidation by DTNB of WT and double cysteine mutant receptors. Changes are measured relative to initial current prior to DTE treatment. Solid lines are joining the two measures for each individual cell.

(D) Summary of the DTE-induced potentiation of WT and double cysteine mutant GluN1/GluN2A NMDARs at interfaces 1, 2 and 3. Mutagenesis positions as well as mean and n values of all panels are given in Appendix Table S1. **P < 0.01, ***P < 0.001, one-way ANOVA on ranks followed by Bonferroni corrected Dunn's test.



Appendix Figure S2: Trapping a rolling motion at the ABD inter-dimer interface results in super-activity both at GluN1/GluN2A and GluN1/GluN2B receptors.

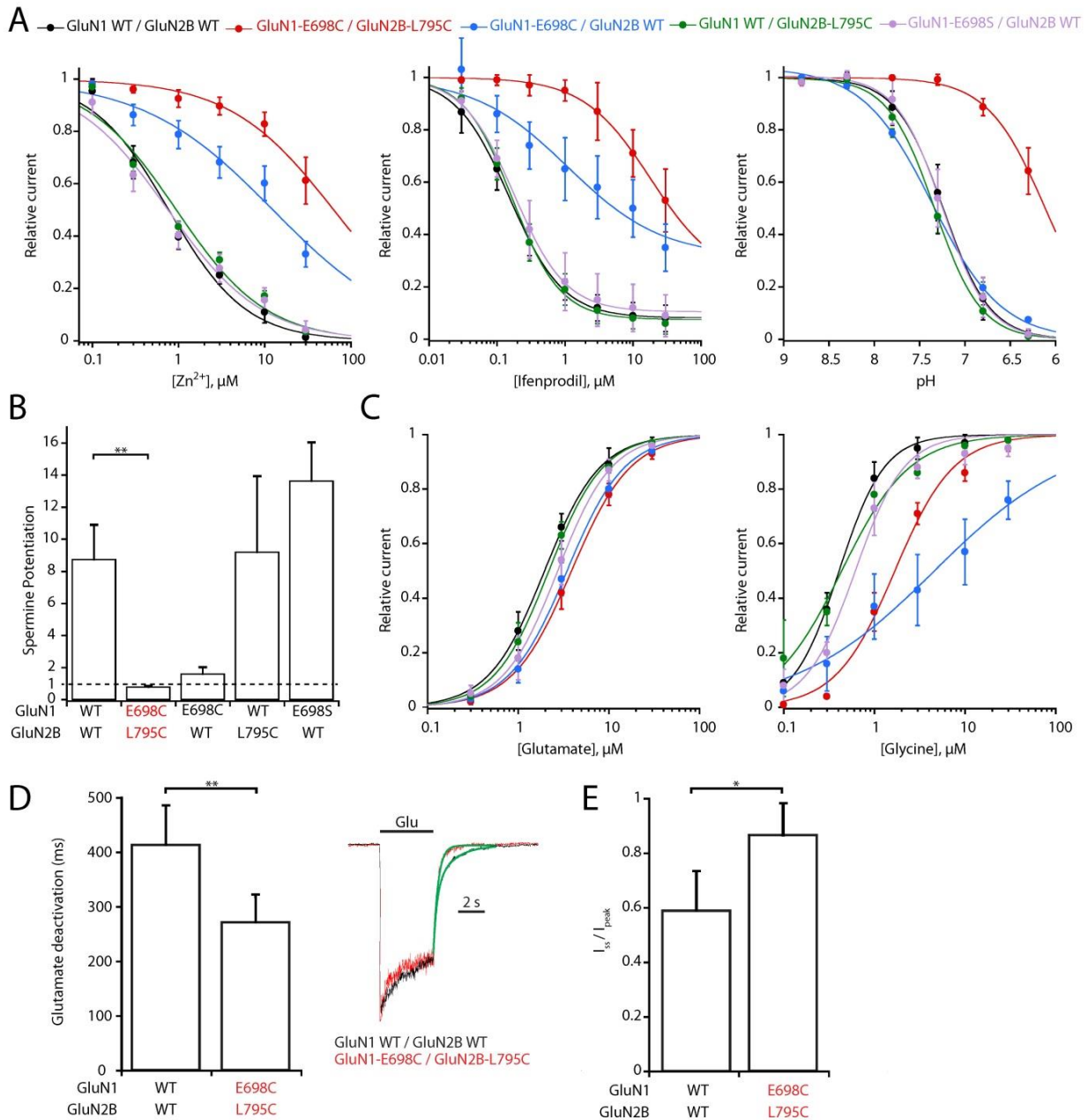
(A) Assessment of receptor channel activity using MK-801 inhibition kinetics in oocyte TEVC experiments. Representative current traces from oocytes expressing WT or the GluN1-E698C/GluN2A-L794C double mutant in response to 10 nM MK-801 during agonist application. Responses were scaled to the current amplitude obtained before MK-801 application. Inset, mono-exponential fits of MK-801 wash-in and wash-out. Note the strikingly faster kinetics in mutant receptors, both at the onset and offset of MK-801.

(B) Relative MK-801 inhibition on- and off-rate constants (k_{on} and k_{off}) obtained from experiments exemplified in panel A.

(C) Assessment of receptor channel open probability in HEK293 whole-cell patch-clamp experiments using MK-801 inhibition kinetics. Representative current traces of 1 μ M MK-801

inhibition of wild-type (WT) GluN1/GluN2A and GluN1/GluN2B receptors, and the corresponding double cysteine mutant receptors GluN1-E698C/GluN2A-L794C and GluN1-E698C/GluN2B-L795C. Mono-exponential fits of MK-801 wash-in kinetics are shown in green. Responses were scaled to the current amplitude obtained before MK-801 application.

(D) Relative MK-801 inhibition on-rate constants (k_{on}) obtained from experiments exemplified in panel C. All values were normalized to the value obtained for the corresponding WT receptors. All values were normalized to the value obtained for WT GluN1/GluN2A receptors. Mean and n values of all panels are given in Appendix Table S2, *P<0.05, **P<0.01, ***P<0.001, one-way ANOVA on ranks followed by Bonferroni corrected Dunn's test. Error bars, SD.



Appendix Figure S3: Super-active GluN1/GluN2B receptors are resistant to NTD-mediated allosteric modulation.

(A) Zinc, ifenprodil and pH dose-response curves of wild-type (WT) and single or double mutant GluN1/GluN2B receptors.

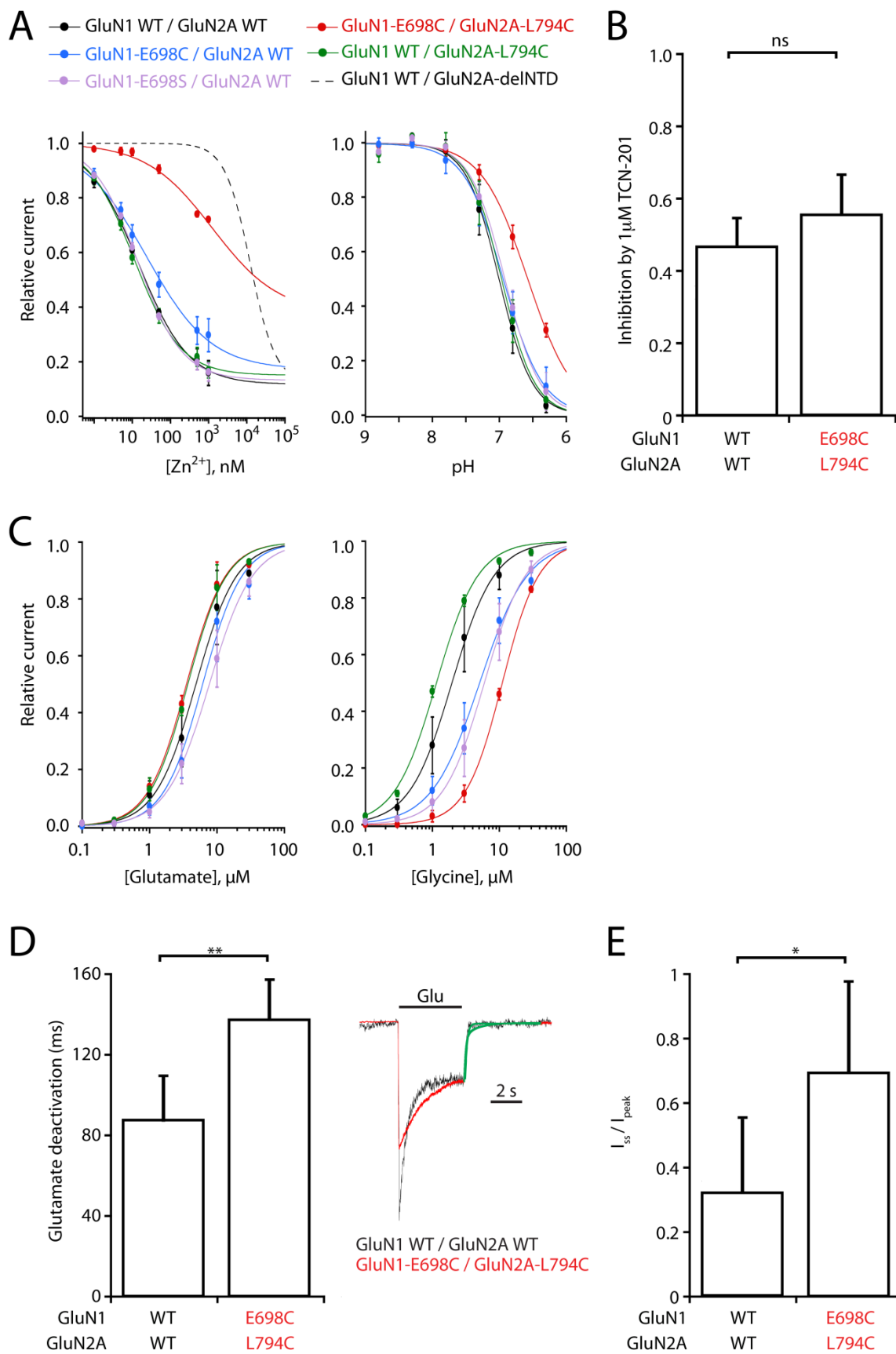
(B) Spermine (200 μM , pH 6.3) potentiation of WT GluN1/GluN2B and single or double mutant GluN1/GluN2B receptors. The first two columns are reproduced from Figure 3C.

(C) Glutamate and glycine dose-response curves of WT and single or double mutant GluN1/GluN2B receptors.

(D) Glutamate deactivation kinetics of WT and double cysteine mutant GluN1/GluN2B receptors ($\tau_{\text{off}} = 414 \pm 69$ ms [n=5] and 272 ± 47 ms [n=6], respectively; **P<0.01, Student's t-test). Right: example current traces normalized to the steady-state current level. Mono-exponential fits of glutamate deactivation kinetics are shown in green. Error bars, SD.

(E) Extent of desensitization of WT and double cysteine mutant GluN1/GluN2B receptors (steady-state over peak current $I_{\text{ss}}/I_{\text{peak}} = 0.59 \pm 0.14$ [n=5] and 0.81 ± 0.12 [n=5], respectively, *P<0.05, Student's t-test). Error bars, SD.

For panel A-C, values of IC_{50} , maximal inhibition (for zinc, ifenprodil and pH), EC_{50} (for glutamate and glycine), Hill coefficient (for all curves), mean (for spermine) and n are given in Appendix Table S3.



Appendix Figure S4: Super-active GluN1/GluN2A receptors are resistant to NTD-mediated allosteric modulation.

(A) Zinc and pH dose-response curves of WT and mutant GluN1/GluN2A receptors. For comparison, the zinc dose-response curve of GluN1/GluN2A receptors lacking the whole GluN2A NTD (GluN1 WT/GluN2A-deINTD) is also shown (dashed lines; data from Rachline *et al.* 2005).

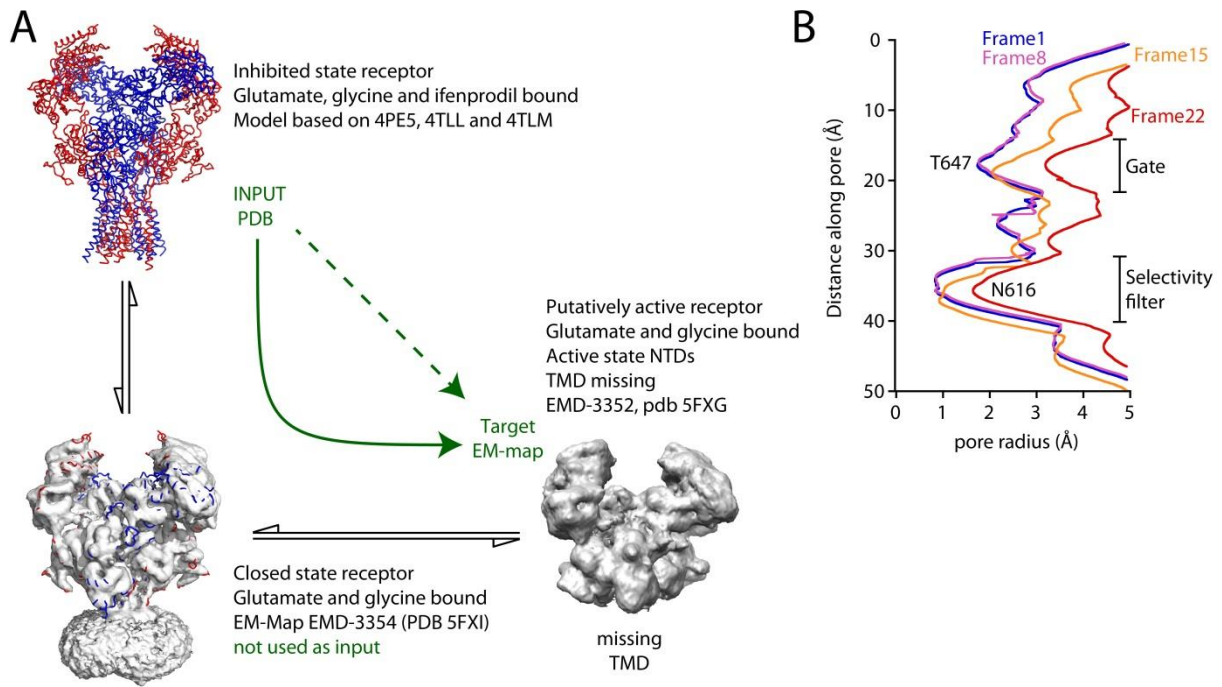
(B) Sensitivity to 1 μ M TCN-201, a GluN2A selective negative allosteric modulator that binds at the ABD level. Note that mutant (n=5) and WT (n=3) receptors display similar TCN-201 sensitivity, thus contrasting with the strong effects seen with NTD-interacting modulators (panel A). P=0.2, Student's t-test.

(C) Glutamate and glycine dose-response curves of WT and single or double mutant GluN1/GluN2A receptors. **P<0.01, one-way ANOVA on ranks followed by Bonferroni corrected Dunn's test. Error bars, SD.

(D) Glutamate deactivation kinetics of WT and double cysteine mutant GluN1/GluN2A receptors ($\tau_{off} = 88 \pm 20$ ms [n=5] and 137 ± 18 ms [n=5], respectively; **P<0.01, Student's t-test). Right: example current traces normalized to the steady-state current level. Mono-exponential fits of glutamate deactivation kinetics are shown in green. Error bars, SD.

(E) Extent of desensitization of WT and double cysteine mutant GluN1/GluN2A receptors (steady-state over peak current $I_{ss}/I_{peak} = 0.32 \pm 0.23$ [n=6] and 0.69 ± 0.27 [n=5], respectively, *P<0.05, Student's t-test). Error bars, SD.

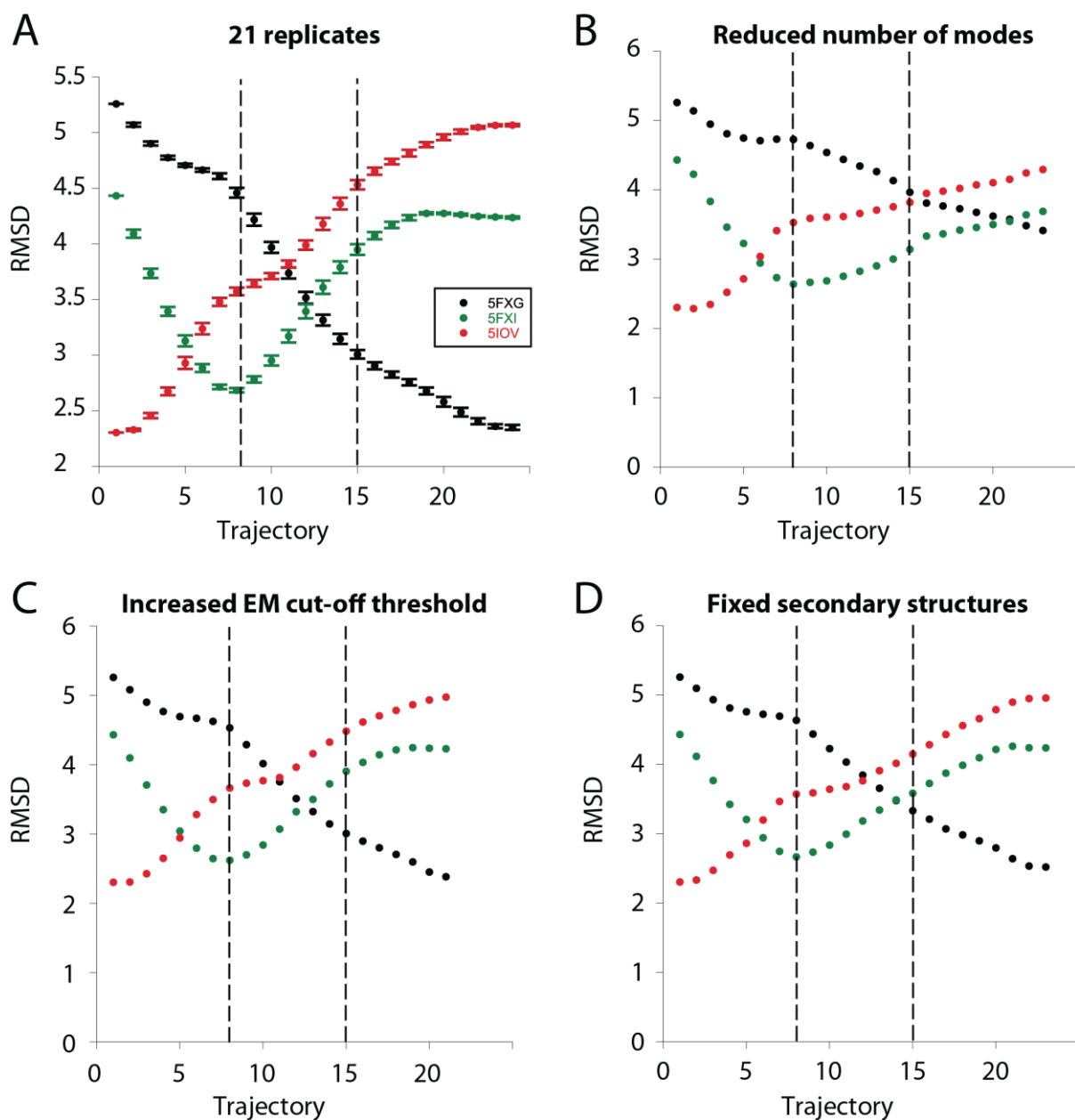
For panels A and B, values of IC_{50} , maximal inhibition (for zinc and pH), EC_{50} (for glutamate and glycine), Hill coefficient (for all curves), and n are given in Appendix Table S3.



Appendix Figure S5: Conformational transitions associated to rolling.

(A) Diagram representing the iMODfit input (inhibited state; top left) for the fitting presented in Figure 4, the 8th frame of the trajectory (bottom left, line representation) inside the EM-Map EMD-3354 (closed state; envelope representation) and the target structure (putative active state, bottom right; envelope representation, TMD not resolved). The good overlap between the 8th frame and the EM-Map 3354 reveals that the iMODFit trajectory passes by this experimentally determined structural state, even though EM-Map 3354 was not fed in the simulation.

(B) Pore radius calculated using HOLE (Smart *et al.*, 1993) at different steps of the iMODFit fitting presented on Figure 4: initial model frame 1 in blue, frame 8 (after step 1) in pink, frame 15 (after step 2) in orange and frame 22 (final frame) in red. Note the large dilation in the upper half of the pore (gate region comprising the M3 SYTANLAAF motif) when transiting through the frames.



Appendix Figure S6: Robustness of iMODfit fitting.

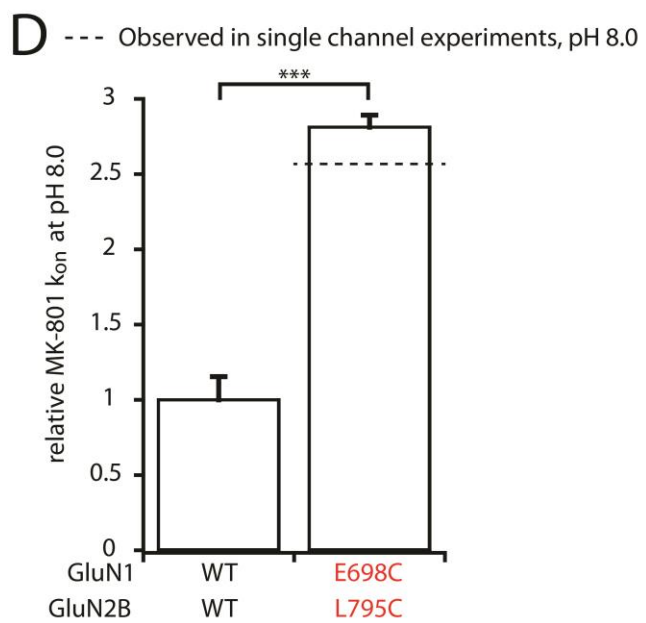
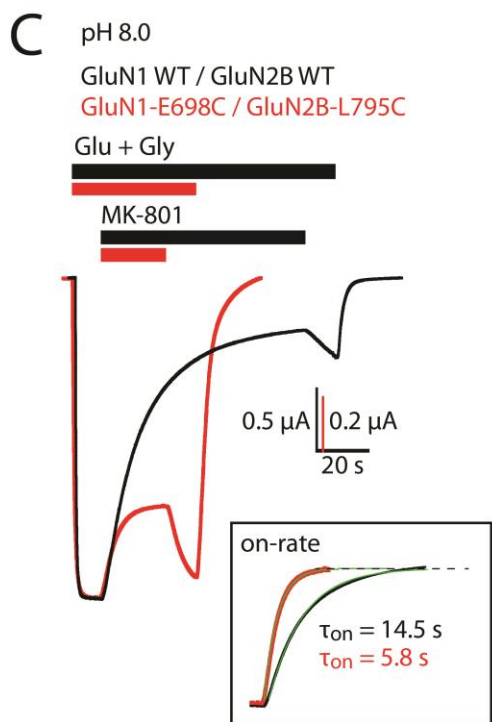
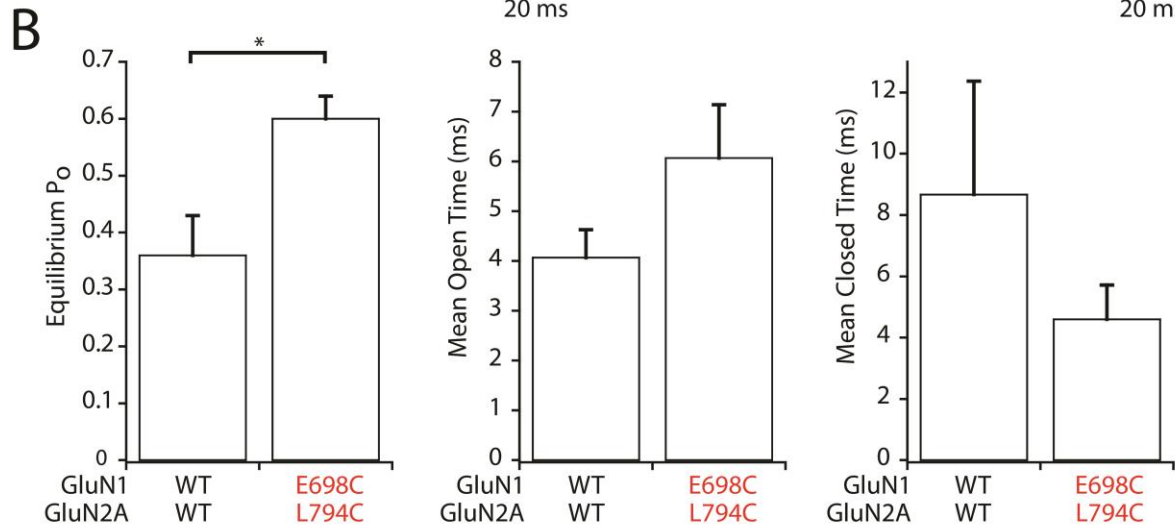
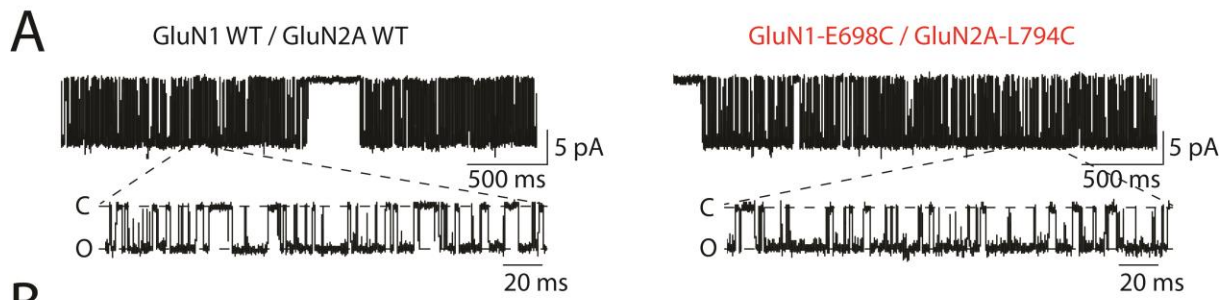
Representation of the evolution of the RMSD of the trajectory calculated against PDBs 5FXG (putative active state) in black, 5FXI (non-active state) in red, and 5IOV (inhibited state) in green over 2267 aligned C α . All trajectories are subdivided in three steps (vertical dashed lines).

(A) Mean trajectories of 21 replicates as shown in Fig 4A. Error bars are SD over the 21 replicates each with different randomization "-- seed" values. Trajectories show minimal difference between replicates. Note that all trajectories pass through the experimentally determined non-active structural structure (pdb 5FXI).

(B) Calculated iMODfit trajectories with lower number of modes per step (-n option; 15 modes per step vs 5% of the modes per step in default parameters as shown in panel A and Fig 4A).

(C) Calculated iMODfit trajectories using a different EM density map threshold (<cutoff> parameter; C=0.045 vs 0.0335 as default parameter).

(D) Calculated iMODfit trajectories fixing secondary elements dihedral (-S option).



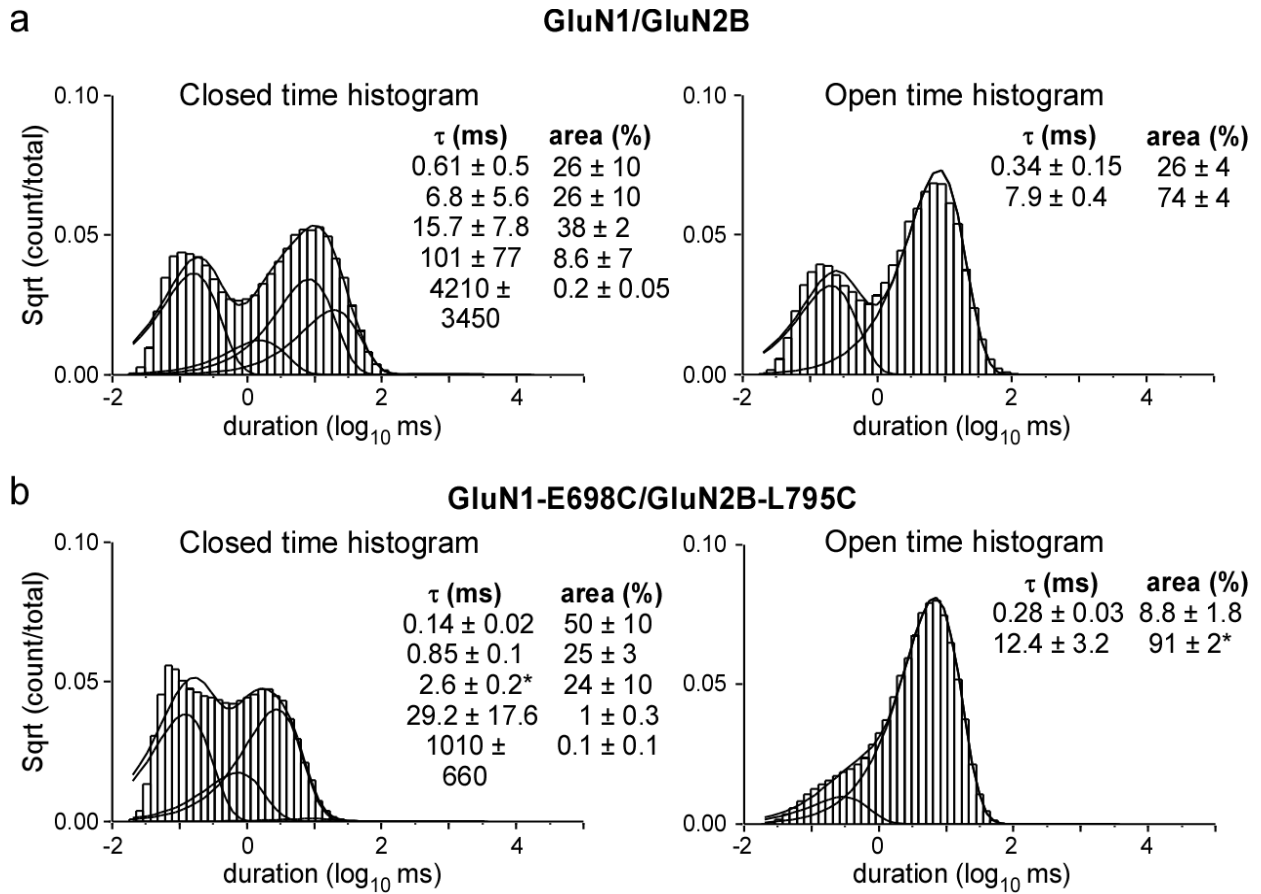
Appendix Figure S7: Super-active receptors at the population and single molecule level.

(A) Representative recordings of patches containing one single wild-type (WT) or GluN1-E698C/GluN2A-L794C receptor. The bottom trace is an expanded view. C, closed channel; O, open channel.

(B) Single channel properties (equilibrium channel open probability, mean open time, mean closed time) of the WT and super-active GluN1-E698C/GluN2A-L794C receptors. Mean and n values are given in Appendix Table S4 * $P < 0.05$, two-tailed Student's t-test, unpaired. Error bars, SEM.

(C) Representative current traces from oocytes expressing either WT or the GluN1-E698C/GluN2B-L795C double mutant receptor in response to 30 nM MK-801 during agonist application at pH 8.0. Responses were scaled to the current amplitude obtained before MK-801 application. Inset, mono-exponential fits of MK-801 wash-in. Note the strikingly faster kinetics in mutant receptors.

(D) Relative MK-801 inhibition on-rate constants (k_{on}) obtained from experiments exemplified in panel c. All values were normalized to the value obtained for WT GluN1/GluN2B receptors at pH 8.0. The change in channel open probability (P_o) measured in single-channel experiments performed at the same pH is shown for comparison (dashed line). Mean and n values are given in Appendix Table S2, *** $P < 0.001$, one-way ANOVA on ranks followed by Bonferroni corrected Dunn's test. Error bars, SD.



Appendix Figure S8: Equilibrium open and closed time distributions for WT and super-active receptors.

Closed (*left*) and open (*right*) durations for GluN1/GluN2B WT (**A**) and GluN1-E698C/GluN2B-L795C receptors (**B**). For all constructs, the closed-time distributions were best fit by five exponentials and the open time distribution by 2 exponentials. *Insets*, mean values (\pm SEM) for closed and open state durations (*left*, τ , ms) and occupancies (*right*, α , %).

Appendix Table S1: Summary of redox treatment effect on NMDAR current amplitude.

Interface	Receptor	DTE Potentiation	n	DTNB reversion	Reversibility
GluN1/GluN2B receptors: double cysteine mutants					
WT	GluN1 WT / GluN2B WT	2.06 ± 0.46	18	1.26 ± 0.18	0.75
1	GluN1-N492C / GluN2B-S188C	120.35 ± 144.15	15	30.20 ± 35.63	0.76
2	GluN1-H162C-D765C / GluN2B WT	121.03 ± 68.20	10	10.02 ± 6.77	0.93
3	GluN1 WT / GluN2B-V195C-M430C	7.15 ± 3.95	16	2.74 ± 1.10	0.72
4	GluN1 WT / GluN2B-N218C	5.47 ± 4.76	8	2.03 ± 2.53	0.70
4	GluN1 WT / GluN2B-K221C	2.03 ± 0.44	8	1.15 ± 0.39	0.85
5	GluN1-R673C / GluN2B-L795C	9.32 ± 5.49	15	2.38 ± 0.99	0.78
GluN1/GluN2B receptor: single cysteine mutants					
1	GluN1-N492C / GluN2B WT	2.46 ± 0.14	6		
1	GluN1 WT / GluN2B-S188C	2.00 ± 0.18	3		
2	GluN1-H162C / GluN2B WT	1.46 ± 0.28	3		
2	GluN1-D765C / GluN2B WT	3.39 ± 0.96	8		
3	GluN1 WT / GluN2B-V195C	2.41 ± 0.94	5		
3	GluN1 WT / GluN2B-M430C	2.30 ± 0.19	3		
5	GluN1-R673C / GluN2B WT	1.14 ± 0.10	6		
5	GluN1 WT / GluN2B-L795C	1.19 ± 0.29	6		
GluN1*/GluN2B receptor (GluN1-C744A-C798A background)					
WT*	GluN1* / GluN2B WT	0.94 ± 0.49	15		
1	GluN1*-N492C / GluN2B-S188C	195.76 ± 78.13	4		
2	GluN1*-H162C-D765C / GluN2B WT	9.12 ± 3.43	4		
3	GluN1* / GluN2B-V195C-M430C	1.03 ± 0.36	14		
4	GluN1* / GluN2B-N218C	3.62 ± 4.00	7		
4	GluN1* / GluN2B-K221C	0.91 ± 0.11	8		
5	GluN1*-R673C / GluN2B-L795C	0.84 ± 0.17	10		
GluN1/GluN2A receptors: double cysteine mutants					
WT	GluN1 WT / GluN2A WT	1.43 ± 0.76	18		
1	GluN1-N489C / GluN2A-T189C	15.21 ± 11.08	9		
2	GluN1-H162C-D765C / GluN2B WT	16.66 ± 6.96	3		
3	GluN1 WT / GluN2B-V196C-T426C	2.14 ± 0.37	4		

Values shown are mean ± SD.

Appendix Table S2: Summary of MK-801 inhibition kinetics experiments.

Receptor	Oocytes TEVC experiments				HEK293 cells patch-clamp experiments	
	Relative k_{on}	n	Relative k_{off}	n	Relative k_{on}	n
GluN1/GluN2B receptors, interface 5						
GluN1 WT / GluN2B WT	1 ± 0.14	22	1 ± 0.13	19	1 ± 0.33	5
GluN1-E698C / GluN2B-L795C	5.38 ± 1.23	24	7.89 ± 2.09	23	5.64 ± 0.93	6
GluN1-E698C / GluN2B WT	1.39 ± 0.49	8	0.82 ± 0.35	6		
GluN1 WT / GluN2B-L795C	1.56 ± 0.52	8	0.92 ± 0.23	5		
GluN1-E698S / GluN2B WT	1.33 ± 0.30	5	1.13 ± 0.31	5		
GluN1/GluN2A receptors, interface 5						
GluN1 WT / GluN2A WT	1 ± 0.16	25	1 ± 0.26	7	1 ± 0.36	5
GluN1-E698C / GluN2A-L794C	1.71 ± 0.35	20	2.04 ± 0.47	6	1.71 ± 0.34	5
GluN1-E698C / GluN2A WT	0.97 ± 0.15	25	1.00 ± 0.33	6		
GluN1 WT / GluN2A-L794C	1.07 ± 0.09	17	1.24 ± 0.32	6		
GluN1-E698S / GluN2A WT	0.87 ± 0.10	6	1.18 ± 0.34	6		
GluN1/GluN2B receptors, interface 1						
GluN1 WT / GluN2B WT	1.00 ± 0.16	7				
GluN1-N495C / GluN2B-N192C	2.10 ± 0.24	7				
GluN1-N495C / GluN2B WT	1.14 ± 0.01	5				
GluN1 WT / GluN2B-N192C	0.58 ± 0.06	5				
GluN1/GluN2B receptors, interface 5, pH 8.0						
GluN1 WT / GluN2B WT	1 ± 0.15	9				
GluN1-E698C / GluN2B-L795C	2.81 ± 0.08	6				

Values shown are mean ± SD.

Appendix Table S3: Summary of pharmacology experiments.

Receptor subtype	Zn ²⁺				Ifenprodil				pH			
	IC ₅₀	I _{max}	n _{Hill}	n	IC ₅₀	I _{max}	n _{Hill}	n	pH ₅₀	I _{max}	n _{Hill}	n
GluN1/GluN2B, interface 5												
GluN1 WT / GluN2B WT	0.77 ± 0.11	fixed to 1	0.97 ± 0.12	4	0.15 ± 0.00	0.92 ± 0.00	1.10 ± 0.02	12	7.24 ± 0.02	1.00 ± 0.01	1.68 ± 0.09	8
GluN1-E698C / GluN2B-L795C	63.07 ± 14.28	fixed to 1	0.72 ± 0.01	5	18.1 ± 4.92	0.77 ± 0.09	0.87 ± 0.06	9	6.11 ± 0.03	1.00 ± 0.01	1.36 ± 0.16	6
GluN1-E698C / GluN2B WT	12.43 ± 2.74	fixed to 1	0.57 ± 0.08	5	1.10 ± 1.05	0.68 ± 0.15	0.63 ± 0.24	14	7.36 ± 0.02	1.04 ± 0.02	1.13 ± 0.06	4
GluN1 WT / GluN2B-L795C	0.94 ± 0.19	fixed to 1	0.83 ± 0.13	5	0.17 ± 0.01	0.92 ± 0.01	1.22 ± 0.08	10	7.34 ± 0.01	1.00 ± 0.01	1.69 ± 0.08	4
GluN1-E698S / GluN2B WT	0.75 ± 0.13	fixed to 1	0.80 ± 0.10	5	0.18 ± 0.01	0.89 ± 0.01	1.14 ± 0.05	7	7.25 ± 0.02	1.01 ± 0.02	1.71 ± 0.13	7
GluN1/GluN2A, interface 5												
GluN1 WT / GluN2A WT	14.65 ± 2.12 [#]	0.88 ± 0.03	0.66 ± 0.05	4					7.00 ± 0.03	1.00 ± 0.02	1.75 ± 0.18	5
GluN1-E698C / GluN2A-L794C	1256.3 ± 4646.5 [#]	0.62 ± 0.62	0.5 ± 0.19	4					6.58 ± 0.01	1.00 ± 0.00	1.26 ± 0.03	7
GluN1-E698C / GluN2A WT	23.41 ± 10.38 [#]	0.83 ± 0.07	0.51 ± 0.08	4					6.94 ± 0.01	1.00 ± 0.01	1.48 ± 0.05	5
GluN1 WT / GluN2A-L794C	11.17 ± 1.11 [#]	0.85 ± 0.02	0.72 ± 0.05	4					6.97 ± 0.03	1.00 ± 0.02	1.75 ± 0.19	5
GluN1-E698S / GluN2A WT	13.821 ± 1.00 [#]	0.86 ± 0.01	0.74 ± 0.04	4					6.92 ± 0.03	1.00 ± 0.02	1.65 ± 0.15	5

Receptor subtype	Spermine		Glutamate			Glycine		
	Mean	n	EC ₅₀	n _{Hill}	n	EC ₅₀	n _{Hill}	n
GluN1/GluN2B, interface 5								
GluN1 WT / GluN2B WT	8.73 ± 2.17	10	1.95 ± 0.07	1.41 ± 0.07	8	0.41 ± 0.02	1.73 ± 0.11	7
GluN1-E698C / GluN2B-L795C	0.78 ± 0.07	9	3.87 ± 0.08	1.33 ± 0.03	6	1.68 ± 0.17	1.33 ± 0.16	4
GluN1-E698C / GluN2B WT	1.60 ± 0.43	7	3.45 ± 0.13	1.36 ± 0.06	7	4.58 ± 0.84	0.56 ± 0.07	7
GluN1 WT / GluN2B-L795C	9.19 ± 4.74	6	2.17 ± 0.08	1.45 ± 0.07	5	0.44 ± 0.05	1.15 ± 0.14	5
GluN1-E698S / GluN2B WT	13.62 ± 2.42	8	2.72 ± 0.06	1.45 ± 0.04	6	0.62 ± 0.07	1.61 ± 0.25	5
GluN1/GluN2A, interface 5								
GluN1 WT / GluN2A WT			4.87 ± 0.33	1.44 ± 0.12	9	1.96 ± 0.08	1.37 ± 0.07	7
GluN1-E698C / GluN2A-L794C			3.52 ± 0.19	1.50 ± 0.11	5	11.06 ± 0.11	1.58 ± 0.02	5
GluN1-E698C / GluN2A WT			6.12 ± 0.56	1.49 ± 0.17	8	5.07 ± 0.28	1.21 ± 0.07	7
GluN1 WT / GluN2A-L794C			3.69 ± 0.16	1.52 ± 0.09	6	1.15 ± 0.06	1.39 ± 0.09	6
GluN1-E698S / GluN2A WT			7.70 ± 0.11	1.36 ± 0.02	7	5.96 ± 0.10	1.40 ± 0.03	5

All IC₅₀ and EC₅₀ values are given in μM except for those marked with # which are given in nM.

Appendix Table S4: Single channel properties of wild type and ABD rolling locked GluN2A- and GluN2B- containing NMDA receptors.

Construct	Total events (# of patches)	<i>i</i> <i>pA</i>	eq. P_{open}	MCT <i>ms</i>	MOT <i>ms</i>
GluN1/GluN2A	511004 (7)	-7.6 ± 0.4	0.36 ± 0.07	8.7 ± 3.7	4.1 ± 0.6
GluN1-E698C/ GluN2A-L794C	295171 (8)	-8.3 ± 0.5	0.60 ± 0.04*	4.6 ± 11.2	6.1 ± 1.1
GluN1/GluN2B	205064 (5)	-7.6 ± 0.3	0.29 ± 0.05	15.8 ± 2.1	6.4 ± 1.3
GluN1-E698C/ GluN2B-L795C	286299 (5)	-6.5 ± 0.3*	0.74 ± 0.07*	5.1 ± 1.9*	14.2 ± 2.4*

Values shown are mean ± SEM for single-channel current amplitude (*i*), equilibrium open probability (eq. P_o), mean closed time (MCT), and mean open time (MOT). Single channel currents were recorded in the on-cell mode at approximately -100 mV and analyzed in QuB (see Materials and Methods). Number of patches is in parenthesis to the right of total events. Eq. P_o is the fractional occupancy of the open states in the entire single-channel recording, including long lived closed states (desensitized states). All data were idealized and fit at a dead time of 20 μ s.

Asterisks (*) indicate values significantly different than their respective wild type ($p \leq 0.05$, two-tailed Student's *t*-test, unpaired).

Appendix Table S5: Cross-link ABD rolling alters activation kinetic rate constants.

		C ₃ -C ₂	C ₂ -C ₁	C ₁ -O ₁	C ₃ -C ₅	C ₂ -C ₄	O ₁ -O ₂
GluN1/	k _f	230±100	530±180	1670±770	40±20	1.2±0.2	2640±930
GluN2B	k _r	230±120	2430±1100	1220±370	11.9±7.8	0.6±0.2	430±60
	K _{eq}	3.3±2.2	0.33±0.12	1.2±0.5	3.6±1.3	3.5±1.7	5.8±1.7
	ΔG	-0.40±0.4	0.75±0.24	0.09±0.37	-0.67±0.22	-0.59±0.30	-0.96±0.23
GluN1- E698C	k _f	610±150	1320±120	4130±460	71±31	3.4±2.4	2420±190
	k _r	240±76	2550±840*	450±90	23±5	4.5±3.6	840±200
GluN2B-	K _{eq}	2.6±0.2	0.60±0.15	9.7±1.4*	3.6±2.1	3.7±1.9	3.2±0.8
L795C	ΔG	-0.57±0.05	0.34±0.15	-1.3±0.1*	-0.52±0.39	-0.03±0.98	-0.66±0.14

Mean values (\pm SEM) for forward (k_f) and reverse (k_r) kinetic rate constants (s⁻¹) for a 5C-2O kinetic scheme (Figure 6). ΔG is in units of kcal/mol. Kinetics models were constructed as C₃-C₂-C₁-O₁-O₂ while C₄ and C₅ branched from C₃ and C₂, respectively (see Material and Methods). C₄ and C₅ reflect desensitized states.